PAPER REF: 4679

STRUCTURAL DESIGN OF A COMPOSITE VARIABLE-SPAN WING

Pedro D.R. Santos[1(*)], Pedro V. Gamboa[1], Pedro M.B. Santos[1], José M.A. Silva[1]
[1]LAETA-UBI/AEROG, University of Beira Interior, Covilhã, Portugal
[(*)]*Email:* p_daniel_santos@hotmail.com

ABSTRACT

This paper addresses the structural design of a composite variable-span morphing wing intended to be installed on a small UAV to provide high flight efficiency in an extended operational speed range, relative to a conventional fixed wing, by symmetrically adjusting the wing span to the flight speed. The design work is divided into three main parts: (1) structural layout definition according to the morphing concept constraints and the materials used; (2) design for static loads using the finite element method (FEM) where strength, stiffness and weight are key design parameters; (3) experimental testing of a prototype of the wing. The results show that the design has good stiffness and strength characteristics and that the numerical predictions correlate well with the experimental tests.

Keywords: composite materials, structural design, variable-span wing.

INTRODUCTION

From an aerodynamics perspective, the overall shape of the wing is the most important design parameter for an aircraft. When a specific type of mission is required, there is usually an ideal configuration of the aircraft to accomplish it (Amador, 2009). This makes the aircraft highly efficient in some flight conditions while reducing the efficiency in others. The objective of morphing wings, such as the variable-span wing, is to mimic the behavior of birds, which adapt their wings to the flight conditions, either a dive to catch a prey or gliding to save energy (Gonzalez, 2005). With the wing fully extended, in a configuration of high lift for takeoffs and landings, the lift-to-drag ratio is improved, as well as the takeoff and landing distances, although at the cost of increased parasite drag. While at cruise or loiter, the wing retracts the outer panels, reducing the wing plan area and aspect ratio, which decreases drag for a more efficient cruise and extra range. This system may require advanced materials, such as advanced piezoelectric materials, advanced fiber optic sensing techniques, fabrication of integrated composite structures (Wlezien, 1998) and new actuation mechanisms. But with the present technology, the mechanisms that would allow this kind of capability are impractical in the sense that the weight of the wing would increase considerably as well as its cost-effectiveness (Gonzalez, 2005). This makes the variable-span wing currently impossible to implement in a manned aircraft. However, it can be implemented in small-scale unmanned aerial vehicles (UAV's), both for military and civil applications, in which the reduced size of the aircraft minimizes the disadvantages and maximizes the advantages. A thorough review of morphing aircraft concepts, which have seen some kind of success in flight (Barbarino, 2011) in terms of functionality, shows that there is a huge effort in the scientific and engineering community to develop efficient and reliable systems.

This paper discusses the structural design of a variable-span wing (VSW) and a finite element model validation developed to model the particular characteristics of the wing with regards to its moving parts. An analysis of de deflections and stresses under aerodynamic flight loads is also presented to assess the suitability of the wing for flight under static conditions.

THE VARIABLE SPAN WING

The shape and size of the variable-span morphing wing (VSW) was obtained through a computational constrained aerodynamic shape optimization aimed at determining the wing chord and span values that minimized its drag for a given speed range. The geometric constraints imposed on the wing design optimization were dictated by component fitting, manufacturing simplicity and mechanism functionality considerations. A detailed description of the aerodynamic optimization procedure and results is given in (Mestrinho, 2011). The actuation mechanism, wing structure and manufacturing techniques used to build the structure of the wing prototype are presented in in detail in (Felício, 2011).

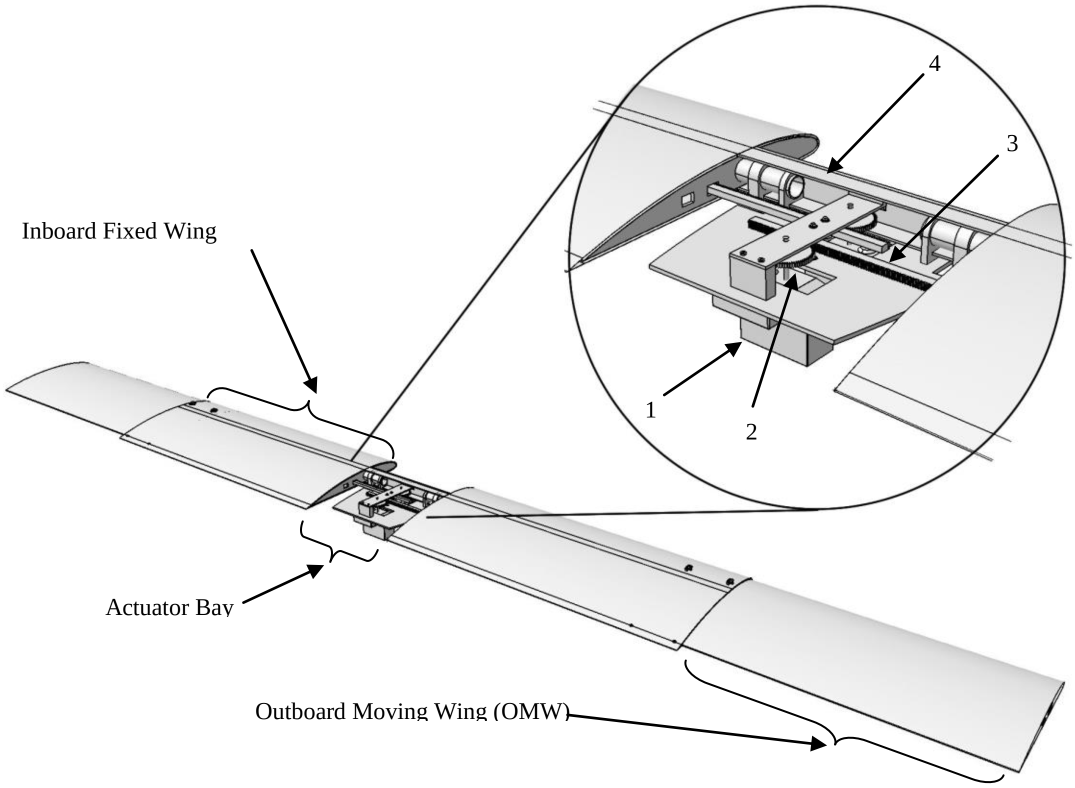

Fig.1 General CAD view of the Variable-Span Wing (VSW) showing its main components and a detail of the actuator bay: (1) servo-motor; (2) transmission pinion; (3) transmission rack; and (4) pultruded unidirectional carbon spar

Wing Concept

The variable-span wing concept in the present work exhibits a very simple layout: a hollow wing, the inboard fixed wing (IFW), inside of which a smaller conventional wing, outboard moving wing (OMW), slides actuated by a simple electromechanical mechanism consisting of a servomotor, a pinion and rack. The maximum span length is 2.5m. For this total span, both inboard and outboard wing parts have a length of 0.625m and a 0.1m of minimum wing overlapping provides sufficient wing stiffness in the full extended configuration. The overall system was developed in a CAD/CAM tool and is illustrated in Fig. 1 where the main components are highlighted.

Both wing parts are of constant chord length which facilitates manufacture and makes the fitting and support of the outboard wing easier to implement. The chord length of the IFW is larger to allow the OMW to fit inside it. Their values are 0.266m and 0.245m, for the IFW and the OMW, respectively.

Materials and Structural Concept

The structural components of the wing were developed with a combination of composite materials and hard and soft wood which provide good general strength and stiffness.

The IFW uses a monocoque type of structure with a sandwich skin of carbon/foam/carbon which is required to both provide the correct shape and resist shear loads. From inside out, the load carrying thick skin has a layer of 48g/m^2 glass/epoxy, a layer of 185g/m^2 carbon/epoxy, a layer of 2mm porous PVC foam (55kg/m^3), a layer of 185g/m^2 carbon/epoxy, and finally another layer of 48g/m^2 glass/epoxy. The PVC foam core was incorporated between the carbon fiber layers to allow embedding of the main spar and to give adequate stiffness to the skin. All fiber fabric layers are plain weave oriented at 0deg along the wing span. The glass layers do not have a structural role but are added to reduce the porosity of the carbon/epoxy layers. The complete assembled skin has a thickness of 2.5mm, which creates a fairly acceptable small discontinuity between the IFW and the OMW. Spar caps inside the IFW are composed of rectangular beams made of pultruded carbon fiber with a cross-section of 16mm$\times$1.7mm. For greater strength and stiffness, the spar extends along the complete fixed wing span of 1.475m. This can be observed in Fig. 1.

The total length of the OMW is 625mm, where 525mm is the stroke and 100mm is the overlap with the remaining IFW so that bending and torsion moments can be effectively transmitted from the OMW to the IFW. The structural configuration used in the moving wing part is very conventional: the wing is composed of ten 2mm thick balsawood ribs, a 240g/m^2 carbon fiber/epoxy skin and a I-section spar consisting of 8mmx0.8mm pultruded carbon spar caps with a 1.5mm balsa wood spar web. The main spar confers sufficient bending stiffness while the ribs provide the correct wing shape. The ribs are bonded to the skin and spar with epoxy glue.

The material properties for the PVC foam, the balsa wood and the pultruded carbon/epoxy were obtained from the manufacturer's datasheets. The woven carbon/epoxy composite elements properties were obtained experimentally following ASTM D3039/D3039M (ASTM, 2000). This standard contains guidelines to determine the ultimate tensile strength of the composite and the longitudinal elastic modulus. Five rectangular carbon/epoxy specimens were hand laminated with a fiber orientation of 0º/90º balanced and symmetric, for which the specified dimensions are 25mm in width, 250mm in length and 1.1mm in thickness. The specimens were tested in a Shimadzu universal testing machine up to rupture, with a test speed of 2mm/min and with the data being recorded in the form of a load/strain curve. The maximum registered load was used to determine the ultimate tensile strength of the specimens and from the curve's slope the elastic moduli, E_1 and E_2, were computed. Since the skin material has identical fiber fractions at 0º a 90º both longitudinal elastic moduli are assumed to be the same. The results were statistically analyzed revealing the sample mean (average), the sample standard deviation and the sample coefficient of variation, in percentage. The individual and statistic results for the ultimate tensile strength and the longitudinal elastic modulus are shown in Tables 1 to 3. The properties of the different materials used in the VSW structure are summarized in Table 4.

Table 1 Specimens' tensile test results

Specimen	Maximum stress F_{tu}, MPa	Elastic Modulus E, GPa
1	594.25	51.58
2	627.95	51.41
3	648.95	52.95
4	640.23	51.39
5	643.33	51.37

Table 2 Specimens' average tensile strength

Average F_{tu}, MPa	Standard deviation, MPa	Coefficient of variation, %
630.94	21.90	3.47

Table 3 Specimens' average longitudinal elastic modulus

Average E, GPa	Standard deviation, GPa	Coefficient of variation, %
51.74	0.68	1.31

Table 4 Material properties

Property	Wooven carbon/epoxy	Pultruded carbon/epoxy	Balsa wood	PVC foam (Airex C70.55)
ρ, kg/m^3	1600	1500	120	55
E_1, GPa	51	120	1.28	0.045
E_2, GPa	51	8	0.0192	0.045
G, GPa	5	5	0.04736	0.022
ν_{12}	0.1	0.3	0.488	0.0227
ν_{23}	0.1	0.3	0.231	0.0227
F_{tu1}, MPa	600	1100	19.9	1.0
F_{tu2}, MPa	600	-	-	1.0
S_{12}, MPa	90	70	1.07	0.7

The cross-sections of the wing are represented in Fig. 2 clearly showing the different structural layouts adopted for the inboard and outboard parts of the wing as necessary to allow the motion of the OMW inside the IFW. The circular tubes in the OMW are present to allow the span actuation system components to move inside it and although they have no special structural function they do increase the stiffness of the OMW both in bending and in torsion.

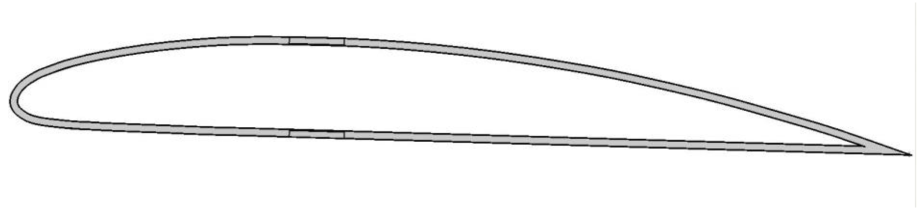

(a)

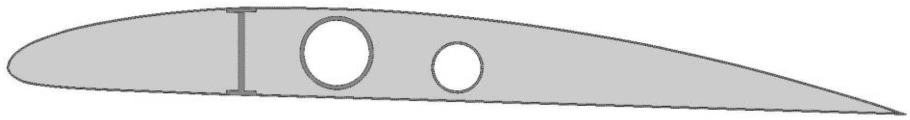

(b)

Fig.2 Wing cross-sections: (a) IFW and (b) OMW

Numerical Model

The numerical model of the VSW wing is developed in ANSYS Mechanical using the *ANSYS Parametric Design Language* (APDL) (ANSYS, 2011) with shell and beam elements according to the model shown in Fig. 2. An APDL script is written to handle geometry creation, material definition, section properties and meshing.

The IFW is discretized using elements SHELL181. The sandwich skin is modeled with three layers built as offset surfaces from the airfoil contour according to its own thickness. These three layers constitute the carbon epoxy and PVC sandwich. In the locations of the embedded spar, the PVC foam layer is replaced with unidirectional pultruded carbon-epoxy. Likewise, the OMW skins, ribs, I-shaped spar web and circular spar are discretized using SHELL181 type elements. The OMW I-spar cap is discretized using BEAM188 elements.

The SHELL181 element is suitable for analyzing thin to moderately-thick shell structures. It is a four-node element with six degrees of freedom at each node: translations in the *x*, *y*, and *z* directions, and rotations about the *x*, *y*, and *z*-axes. This type of element is well-suited for linear, large rotation, and/or large strain nonlinear applications. Additionally, the change in shell thickness is taken into account in nonlinear analyses. The BEAM188 is suitable for analyzing slender to moderately thick beam structures. The element is a linear, quadratic, or cubic two-node beam element in 3D. BEAM188 has six degrees of freedom at each node. These include translations in the *x*, *y*, and *z* directions and rotations about the *x*, *y*, and *z* directions. This element is well-suited for linear, large rotation, and/or large strain nonlinear applications.

The peculiar structure used by the VSW, required the use of contact elements, in order to correctly model the interface. This contact in the overlap surface between the IFW and the OMW is modeled with a shell to shell contact using TARGE170 (target element for 3D geometries) and CONTA173 (contact element for 3D shells without mid side nodes). Since the distinction between the contact and target surfaces is not clear in the interface, a symmetric contact (or "two-pass contact") is created. In this type of contact, each surface is designated to be both a target and a contact surface. Then, two sets of contact pairs between the contacting surfaces are generated. The symmetric contact is less efficient than asymmetric contact. One other reason to use this type of contact in this particular situation is to reduce penetration between contact surfaces. Throughout the work two types of behavior of the contact elements are used: standard and bonded (always bonded option). The former is used when the flexible contact is required on the interface. The latter, as the name infers, is used to simulate a rigid connection of the interface.

The wing is considered to be built-in near the root vicinity. Additionally, the center portion of the inner most rib of the OMW is constrained along the *y*-axis to simulate the constraint imposed by the rack and pinion actuator mechanism and thus avoid outward sliding of the OMW. Figure 3 shows the different assemblies that compose the FE model, as well as the complete assembled finite element model.

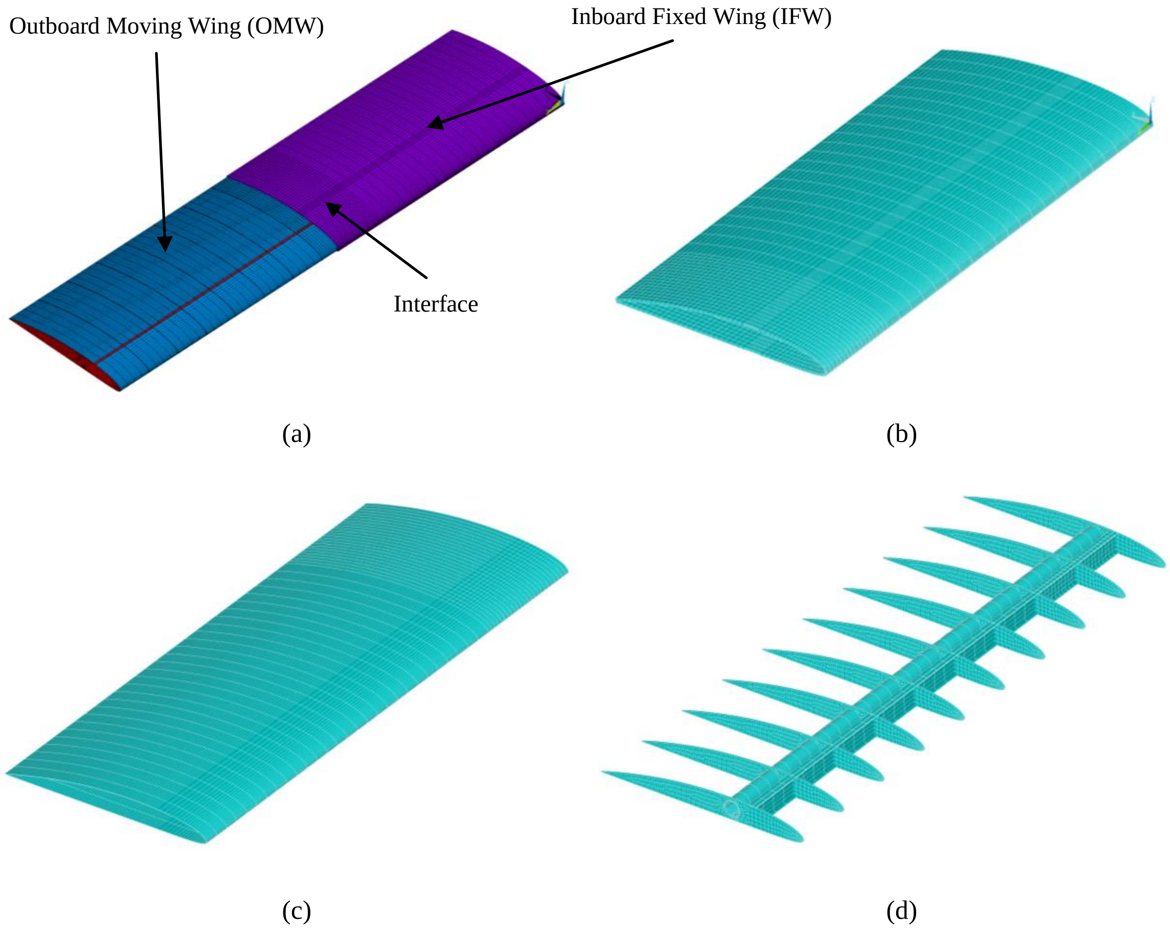

Fig.3 Variable-span wing model in ANSYS Mechanical APDL: a) complete finite element model, b) IFW layered shell, c) OMW shell and d) OMW ribs, I-beam and circular spar.

Mesh Convergence Study

A convergence analysis of the finite element model is carried out to assess the sensitivity of the maximum tip deformation as a function of the number of elements in the grid. Several grid meshes were created and a static analysis is performed with a uniformly distributed load along the span. During this study, the contact between the IFW and OMW is considered to be bonded.

The refinement of the grid mesh was done by changing the default element size in ANSYS. Figure 4 shows the convergence of the maximum wing tip defection for several mesh grids. It is possible to conclude that the solution is for practical reasons stabilized for a grid with about 31000 elements. In fact, the deflection variation is well below 1%. Therefore, the finite element model with 31000 elements is selected for the following analysis.

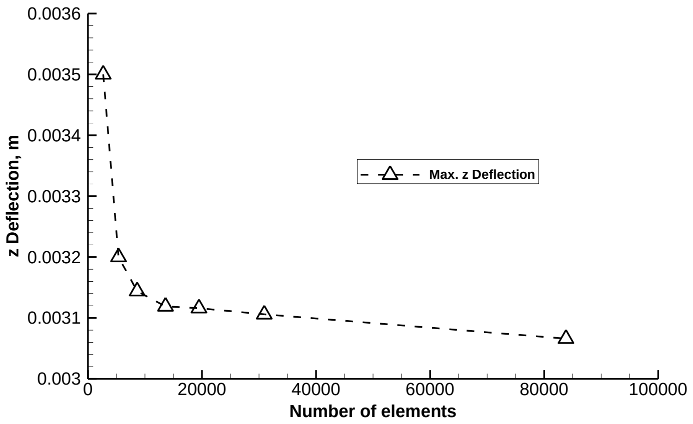

Fig.4 Maximum tip deflection obtained using different numbers of elements

Experimental Model

The wing prototype illustrated in Fig. 5 has been initially developed not only for proof-of-concept in terms of actuation, structural strength (Felício, 2011) and flight performance but also to statically validate the numerical structural model implemented in this work. Correct information on the stiffness and mass properties of the wing is important to accurately model the dynamics of the wing before it is flown.

Fig.5 Wing prototype during the building process

Bending moments from the OMW are transmitted to the IFW by a minimum of 0.1m overlap when the OMW is fully extended. At this condition, these moments tend to alter the IFW section at the interface because the sandwich skin bends, effectively increasing the section thickness in this region. This effect, arising from the fact that there is no internal structural elements, such as ribs or a spar web, to prevent the deformation, results in reduced bending stiffness at the IFW and OMW interface. This situation produces a flexible interface in bending.

RESULTS AND DISCUSSION

In both experimental tests and numerical analysis, the VSW in the fully extended condition is clamped at its root and is statically tested with two loading cases. These two pairs of test and simulation cases serve to validate the numerical model for the required flight load conditions analysis and to perform aeroelastic studies in other parallel work.

Finite Element Model Validation

In order to assess the numerical model correctness and similarity with the experimental built wing, an experimental setup is implemented. In this setup, the variable-span wing with the span fully extended was clamped at its root and was statically tested with two loading cases: (a) bending with a concentrated load of 5N applied at 35% of the OMW tip chord and (b) torsion with one couple of 1.1Nm at the IFW tip chord. For the former loading case, both experimental and numerical deformations are evaluated at constant 35% chord position along the wing span. In the other loading case, the deformations are evaluated along the IFW tip chord. The results from the numerical study and the experimental tests are shown in Fig. 6.

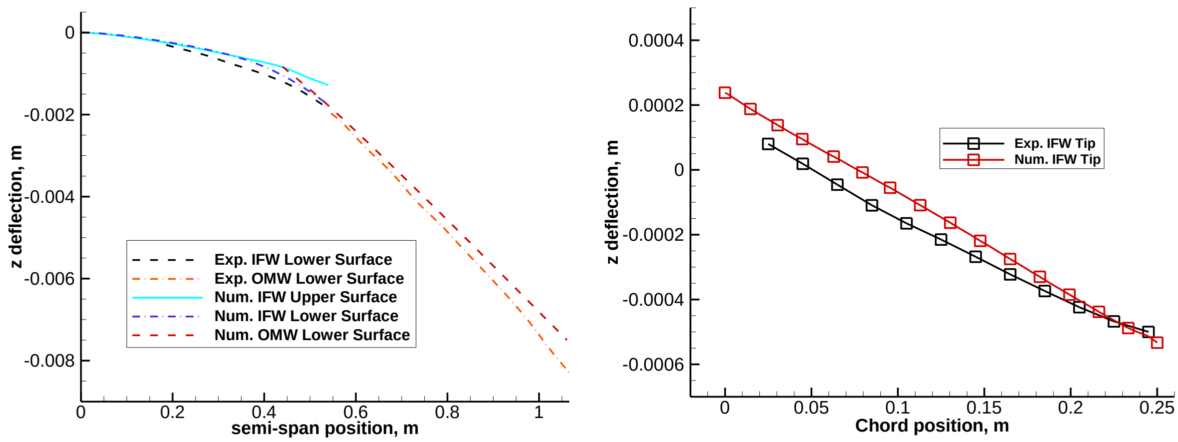

(a) (b)

Fig.6 Static deflections of the variable-span wing: (a) bending along span due to tip load and (b) torsion due to tip couple on IFW tip chord.

Observing Fig. 6(a), which presents the bending along the span due to tip load, it is obvious that a general good agreement exists between experimental and numerical data. It is important to note the change of slope of the deflected shape at the OWM/IFW interface. In fact, the IFW airfoil contour in the proximity of the interface expands and a small gap appears on the top side of the IFW, resulting in the slope discontinuity observed in this region. However, the interface in the numerical model appears to be slightly stiffer, since the maximum deflection is underestimated. Also it is noticeable the high stiffness of the OMW, evidenced by the linear deformation of this component.

Regarding the torsion due to the tip couple (Fig. 6(b)), it is possible to conclude that the torsion angle is similar in both the numerical and the experimental situations. This indicates that the torsional stiffness of the FE model is correct. The differences observed could be related with the precision of the experimental installation (caliper precision and positional error). From both tests, it becomes evident that the developed finite element model represents with good approximation the built wing elastic characteristics.

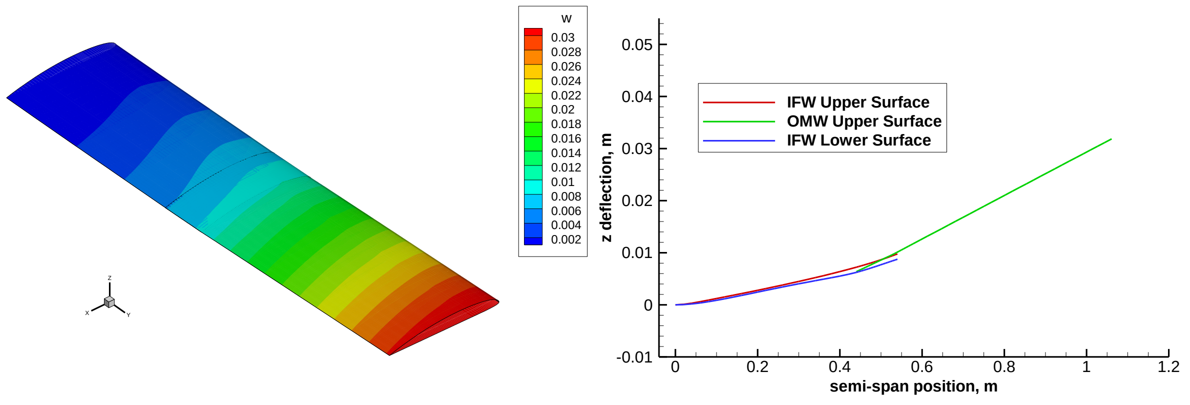

(a) (b)

Fig.7 Deflections of the variable-span wing due to aerodynamic loading of 4G: (a) *z* deflection distribution and (b) *z* deflection along span at 35% chord line.

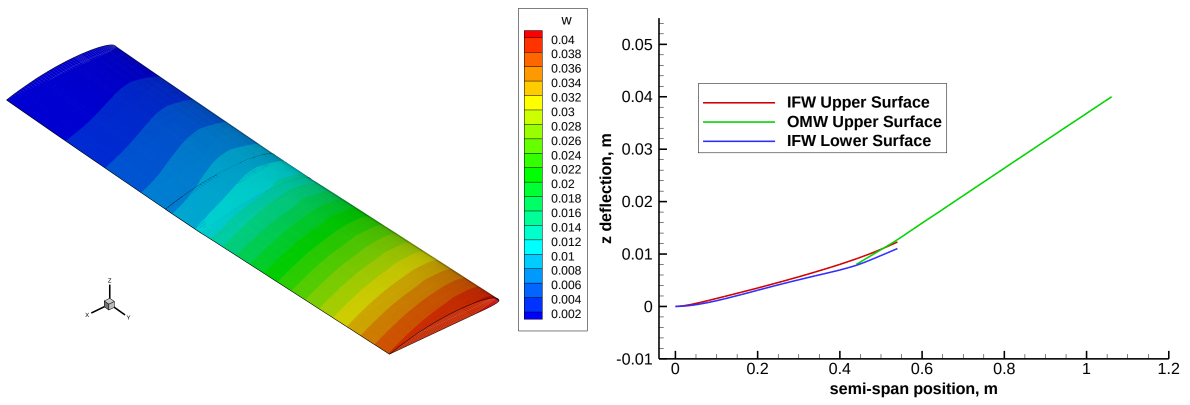

(a) (b)

Fig.8 Deflections of the variable-span wing due to aerodynamic loading of 5G: (a) *z* deflection distribution and (b) *z* deflection along span at 35% chord line.

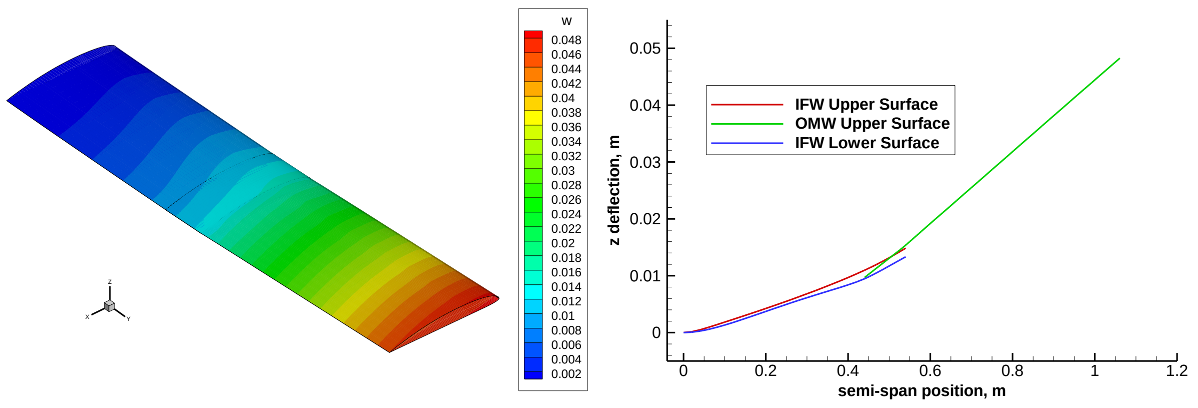

(a) (b)

Fig.9 Deflections of the variable-span wing due to aerodynamic loading of 6G: (a) *z* deflection distribution and (b) *z* deflection along span at 35% chord line.

Aerodynamic Loading Analysis

In order to enhance the knowledge about the performance of the developed structure, the wing deformation induced by aerodynamic loading with varying load factor is studied. More particularly, three loading factors are considered, 4, 5 and 6, corresponding to total lift forces of 120N, 150N and 180N, respectively, on a single wing for a takeoff weight of 60N. The loading is considered to have an elliptic shape and is applied along the span at 25% chord position. The deflections obtained from this study are shown in Figs. 7 through to 9. From all three figures, the widening of the wing thickness at the IFW tip due to the moment transmitted from the OMW is clearly seen. The tip deflection varies from 0.032m at the 4G condition to 0.048m at the 6G load case, corresponding to relative deflections with respect to half-span of 2.6% and 3.8%, respectively. These values are well below the maximum relative deflection of 10% typically allowed in wing designs, but necessary to allow the seamless motion of the OMW under high loads.

For the maximum load factor case, the maximum stress index distribution, from the maximum strength criteria, is obtained to visualize the high stress concentration areas which may require further attention in the structural elements design and to identify oversized areas that can be subject of weight reductions for increased structural efficiency. As expected, two highly stressed regions stand out in Fig. 10: the OMW leading edge skin in the IFW/OMW overlap region and upper and lower rib area on the second and first ribs of the IFW in the same IFW/OMW interface region. The maximum stress index reaches values near 1.0 in these balsa ribs. When the OMW deflects under load, the bending moment transmitted from the OMW to the IFW should produce a linear reaction force distribution over the 0.1m overlap distance, should the structure be completely rigid. However, the effect observed in Fig. 9(b), where the upper and lower skins slightly move apart at the IFW tip chord, makes this reaction distribution to be non-linear and have peak values at the overlap extremities (OMW root chord and IFW tip chord). This effect overloads the lower part of the first OMW rib and the upper part of the second OMW rib due to the vertical compressive reaction that is exerted on them by the IFW sandwich skin. The maximum stress index observed on the leading edge of the IFW in the interface area is close to 0.5, therefore not critical, but results from bending of the leading edge skin as the upper and lower IFW skin move apart in the interface.

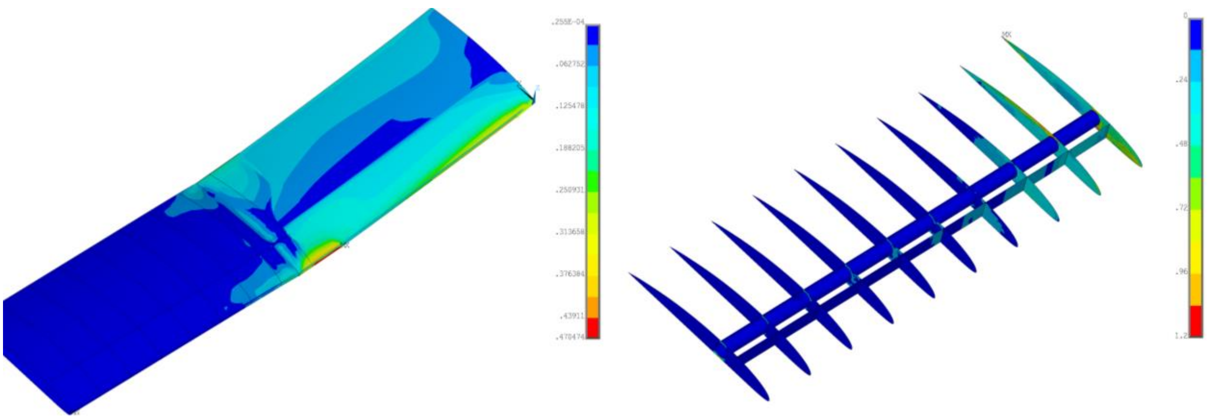

(a) (b)

Fig.10 Maximum stress index distribution of the variable-span wing structure due to an aerodynamic load of 6G (180N): (a) IFW and OMW skin and (b) OMW spars and ribs.

Overall, the wing structure exhibits adequate strength requiring, though three improvements to make it more efficient: (a) increasing the width of the first two balsa ribs of the OMW to reduce the stress levels; (b) stiffening the rib contour at the tip of the IFW to reduce the airfoil section deformation; and (c) reducing the weight of the OMW towards the tip.

CONCLUSIONS

A structural finite element model of a newly developed variable-span wing was developed with ANSYS Mechanical APDL. The model served to study the effect of the interface between the inner fixed part and the outboard moving part of the wing because it is unconventional due to its sliding characteristics. The model was validated with experimental testing of a full-size wing prototype.

This study shows that there is good agreement between the FEM simulation and the experimental deflections of the variable-span wing subjected to the selected loading conditions. Further designs of telescopic wings evolving from this one can thus be performed with the approach used herein.

Static aerodynamic loading conditions were also analyzed for various flight load factors. Deflections and stresses resulting from the load distributions applied show that the structure of the wing is suitable for the flight loads which will be experienced during normal operation.

Further studies, in particular flight testing, will be performed to evaluate the dynamic characteristics of the wing under aeroelastic phenomena, in particular flutter.

ACKNOWLEDGMENTS

The work presented herein has been partially funded by the European Community’s Seventh Framework Programme (FP7) under the Grant Agreement 314139. The CHANGE project (Combined morphing assessment software using flight envelope data and mission based morphing prototype wing development) is a Level 1 project funded under the topic AAT.2012.1.1-2. involving 9 partners. The project started on August 1st 2012.

REFERENCES

Amador MB, Kulkarni V. Morphing Wing Design for UAVs: A Proposed Concept. BSc Thesis, Department of Mechanical and Industrial Engineering, University of Toronto, 2009.

ANSYS® Academic Research, Release 14.0, Mechanical APDL Structural Analysis Guide, Chapter 9, ANSYS, Inc. 2011.

ASTM D3039/D3039M, “Standard Test Method for Tensile Properties of Polymer Matrix Composite Materials”, Book of Standards, 15.03, ASTM International, West Conshohocken, 2000.

Barbarino S, Bilgen O, Ajaj R, Friswell M, Inman D. A review of Morphing Aircraft. Journal of Intelligent Material Systems and Structures, 2011, 22, p.823-877.

Felício J, Santos P, Gamboa P, Silvestre M. Evaluation of a Variable-Span Morphing Wing for a Small UAV. 52th AIAA/ASME/ASCE/AHS/ASC Structures, Structural Dynamics and Materials Conference, Denver, Colorado, 4-7 April, 2011.

Gonzalez L. Morphing Wing Using Shape Memory Alloy: A Concept Proposal. Final research paper in 2005 Summer Research Experience for Undergraduates (REU) on

Nanotechnology and Materials Systems, Texas Institute of Intelligent Bio-Nano Materials and Structures for Aerospace Vehicles (TiiMS) – NASA Research University, Texas A&M University, College Station, Texas, USA, July 2005.

Mestrinho J, Gamboa P, Santos P. Design Optimization of a Variable-Span Morphing Wing for a Small UAV. 52th AIAA/ASME/ASCE/AHS/ASC Structures, Structural Dynamics and Materials Conference, Denver, Colorado, 4-7 April, 2011.

Wlezien RW, Homer GC, McGowan AR, Padula SL, Scott MA, Silcox RJ, Simpson JO. The Aircraft Morphing Program. 39th Structures, Structural Dynamics, and Materials Conference and Exhibit, Long Beach, CA, 20-23 April, 1998.